ChemPubSoc Europe

DOI: 10.1002/celc.201600763

CHEMELECTROCHEM Communications

Electrochemical Infilling of $CuInSe_2$ within TiO_2 Nanotube Layers and Subsequent Photoelectrochemical Studies

Sayantan Das,[a] Hanna Sopha,[a] Milos Krbal,[a] Raul Zazpe,[a] Veronika Podzemna,[a] Jan Prikryl,[a] and Jan M. Macak*[a]

Anodic self-organized TiO_2 nanotube layers (with different aspect ratios) were electrochemically infilled with $CuInSe_2$ nanocrystals with the aim to prepare heterostructures with a photoelectrochemical response in the visible light. The resulting heterostructure assembly was confirmed by field-emission scanning electron microscopy (FESEM), transmission electron microscopy (TEM), and X-ray diffraction (XRD). High incident photon-to-electron conversion efficiency values exceeding 55% were obtained in the visible-light region. The resulting heterostructures show promise as a candidate for solid-state solar cells.

Nanotubular arrangements of titanium dioxide (TiO_2) combined with a high surface area and exceptional optoelectronic properties, have attracted widespread attention as they can be extensively used in the field of photovoltaics, and photocatalysis due to their low cost, non-toxicity, high chemical stability, a long lifetime of photo-generated carriers, and strong catalytic activity.[1] TiO_2 nanotubular layer structures with particular diameters and thicknesses can be grown on Ti substrates by careful optimization of the anodization conditions.[2] The self-organized TiO_2 nanotube layer possess high surface area and enhanced light absorption[3] and belongs to most versatile and best performing TiO_2 structures. However, the wide bandgap of TiO_2 (3.2 eV) limits its photoelectrochemical application in the UV region (representing only 3% of the solar spectrum).[3] Thus to access the visible region, two different strategies have been employed by researchers: 1) doping, and 2) sensitization of TiO_2. In the bulk doping approach, main group elements like carbon,[4] nitrogen[5] or sulphur[6] were introduced into the TiO_2 lattice resulting in the formation of intra-bandgap donor and acceptor levels. In the second approach the TiO_2 nanotube layers are sensitized with visible light absorbing chromophores (like organic dyes[7]) or decorated with quantum dots.[8]

[a] Dr. S. Das, Dr. H. Sopha, Dr. M. Krbal, Dr. R. Zazpe, Dr. V. Podzemna, J. Prikryl, Dr. J. M. Macak
Center of Materials and Nanotechnologies
Faculty of Chemical Technology
University of Pardubice
Nam. Cs. Legii 565, 53002 Pardubice (Czech Republic)
E-mail: jan.macak@upce.cz

There are certainly some drawbacks of organic dyes regarding their stability,[9] whereas cadmium based quantum dots are environmentally unwanted.[10] Recently, a lot of research has been focused on utilizing cadmium free inorganic small band-gap semiconductor to substitute organic dyes and cadmium based materials.[11] Among the inorganic semiconductor materials, ternary I–II–VI_2 chalcopyrite semiconductor materials, such as $CuInSe_2$ (CIS), are very promising materials in the field of photovoltaics, and have been the theme of intense research because of their unique structural and electrical properties.[12] Apart from being a direct band gap energy material with band energy (1.1 eV), CIS also demonstrates good radiation stability, and has a high absorption coefficient ($\approx 10^5$ cm^{-1}).[13] Unlike other absorber materials like CdTe, CIS consists of environmentally benign materials.

The heterojunction between CIS and TiO_2 nanotube layers has been utilized in several reports for the photocatalytic degradation of dyes[14] and organic materials[15] as well as a photocatalyst for hydrogen evolution.[16] Within these reports, TiO_2 nanotubes have been decorated by small CIS quantum dots, nanocrystals or nanospheres utilizing SILAR technique, solvothermal technique or colloidal synthesis.[14–16] The electrochemical deposition represents another viable and low-cost approach to fill or decorate nanotubes.[17] In general, the electrodeposition technique gives close binding between semiconductors, and has often been used in the fabrication of heterojunction electrodes.[17,18] Electrochemical deposition of CIS nanocrystals within TiO_2 nanotubes (layer thickness ≈ 2 μm) has been shown by Wang et al.[19] However, they neither carried out photoelectrochemical, nor any photocatalytic studies. All in all, there is no report on electrodeposited CIS within TiO_2 nanotube layers toward solar cell applications.

Therefore, we demonstrate for the first time the preparation of 1-D heterostructure based on TiO_2 nanotube layers of two different thicknesses (≈ 1 μm and ≈ 6 μm) infilled with visible light absorbing CIS nanocrystals by electrodeposition for an efficient photo-electrochemical light to electricity conversion towards utilization in solid-state solar cells.

Figures 1a and 1b show scanning electron microscopy (SEM) images of Ti/TiO_2(1 μm) and Ti/TiO_2(6 μm) nanotube layers used in this work. These layers were prepared by anodization of titanium foils under specific conditions (see Experimental part for details). Analysis of SEM images (top view and cross-sectional view) revealed that the average diameter (d) and the length (l) of the nanotubes were ≈ 100 nm (d) and ≈ 1 μm (l), and ≈ 230 nm (d) and ≈ 6 μm (l), respectively. Figure 1c displays the SEM image of CIS nanocrystals electro-

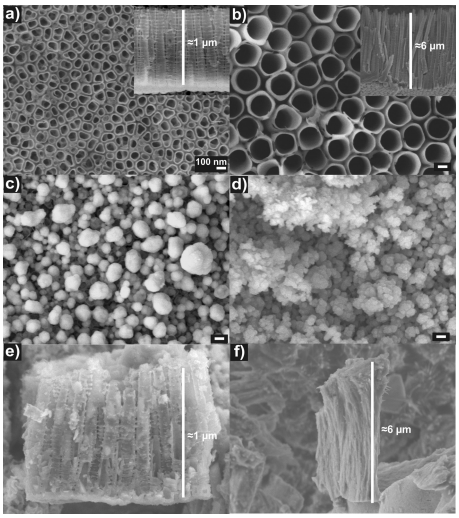

Figure 1. SEM top-view images of: a) Ti/TiO_2(1 μm) and b) Ti/TiO_2(6 μm) nanotube layers; c) Ti/TiO_2(1 μm)/CIS nanotube layers before selenization and d) after selenization. The insets show cross-sectional images. All scale bars show a distance of 100 nm. Cross-sectional images of e) Ti/TiO_2(1 μm)/CIS and f) Ti/TiO_2(6 μm)/CIS nanotube layers after selenization show fully preserved layers.

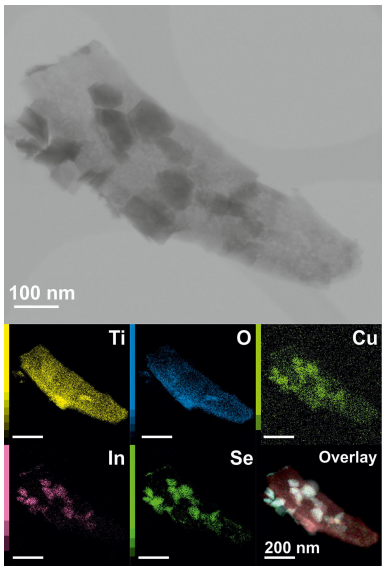

Figure 2. TEM image and elemental mapping of a fragment of single Ti/TiO_2 (6 μm)/CIS nanotube.

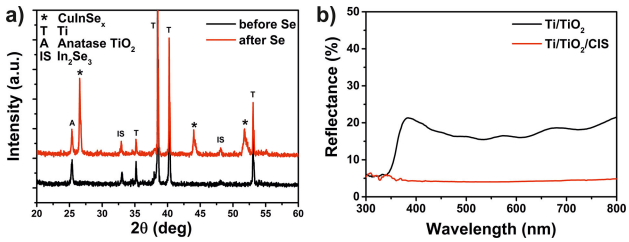

Figure 3. a) XRD patterns of Ti/TiO_2(1 μm)/CIS nanotube layers before and after selenization; b) diffused reflectance spectra of Ti/TiO_2(1 μm) and selenized Ti/TiO_2(1 μm)/CIS nanotube layers.

deposited within the Ti/TiO_2(1 μm) nanotube layers. It was found that electrodeposition resulted in quick infilling of the nanotube with nanocrystals of CIS, scattered on the surface of the nanotube layer. In the course of electrodeposition, CIS nanocrystals (with an average diameter well below 100 nm) were formed inside individual nanotubes, as well as on the surface of the nanotube layer. Figure 1d shows that selenization resulted in complete coverage of the nanotube surface, and the layers became denser when compared to the as-electrodeposited state.

Electrodeposition of CIS within the Ti/TiO_2(6 μm) nanotube layers and subsequent selenization resulted in exactly the same features as shown in Figures 1c and 1d, except that a longer electrodeposition time was required (1560 s). The TiO_2 nanotube layers after CIS infilling and selenization completely preserved their nanotubular shape, as demonstrated via cross-sectional images in Figures 1e and 1f.

To further demonstrate successful infilling of CIS nanocrystals within TiO_2 nanotube layers, TEM and EDX analyses were carried out. Figure 2 illustrates a bright field transmission electron microscope (TEM) image of a single Ti/TiO_2(6 μm)/CIS nanotube fragment, and the elemental mapping of the TiO_2 nanotube. Overall, the TEM studies revealed that CIS nanocrystals were well distributed within the nanotubes, and well attached to the TiO_2 nanotubes, which is essential for the electron transfer process.

Figure 3a shows the x-ray diffraction (XRD) patterns of as-electrodeposited Ti/TiO_2(1 μm)/CIS nanotubular structures before and after selenization. The XRD patterns revealed that selenization is an important step for inducing crystallinity of CIS[20] within the TiO_2 nanotube layers, and a key step for improving the photoelectrochemical properties of the whole nanotubular heterostructure. Moreover, it leads to a better anchoring of CIS to TiO_2 nanotubes. The peaks marked with an asterisk (*) represent the crystalline CIS structure. The XRD patterns following selenization at 450 °C demonstrated the preferred orientation at $2\theta \approx 26.5^\circ$ corresponding to the (112) planes, with the presence of other peaks at $2\theta \approx 44.1^\circ$ and $2\theta \approx 51.8^\circ$ corresponding to the (220) and (312) planes, respectively. It must be noticed here that the anatase peak intensity before and after the selenization remains the same indicating the structural integrity of the TiO_2 nanotube layers. Evaluation of XRD data further revealed a by-product of the electrodeposition corresponding to In_2Se_3. Diffused reflectance spectra of Ti/TiO_2(1 μm), and selenized Ti/TiO_2(1 μm)/CIS nanotube layers, were compared in Fig. 3b. Apparently the bare Ti/TiO_2 nanotube layers (without any CIS nanocrystals) absorb only in the UV region, whereas the Ti/TiO_2(1 μm)/CIS nanotube layers absorb throughout the UV and visible region, and only about 5% is reflected. This confirms very favourable light absorption properties of nanotubular layers with electrodeposited and selenized CIS electrodeposited nanocrystals.

The incident photon-to-current efficiency (*IPCE*) vs wavelength spectra of Ti/TiO_2 and Ti/TiO_2/CIS electrodes were recorded and compared in Fig. 4a and 4b for both tube layers thicknesses.

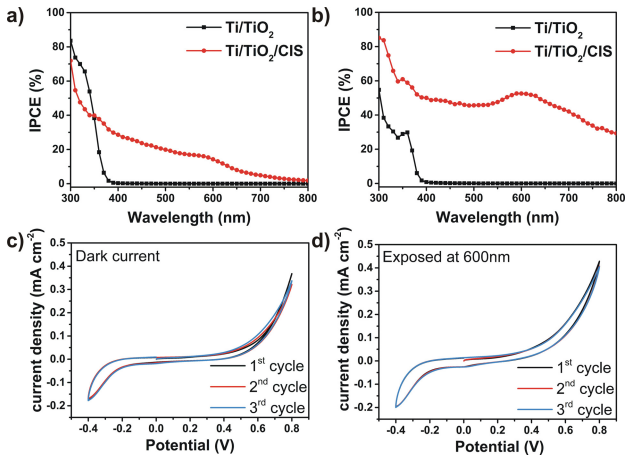

Figure 4. *IPCE* spectra of a) Ti/TiO_2(1 μm)/CIS and b) Ti/TiO_2(6 μm)/CIS nanotube layers compared with the corresponding blank nanotubes (without CIS). Cyclic voltammetry (CV) results of Ti/TiO_2(1 μm)/CIS recorded under c) dark and d) VIS light (wavelength 600 nm) conditions. All curves were recorded in 0.1 M aqueous Na_2SO_4 electrolyte; results in (a) and (b) were obtained at 0.4 V vs. Ag/AgCl.

The TiO_2 nanotube layers infilled with CIS nanocrystals showed enhanced photocurrent response in the visible range, in contrast to bare Ti/TiO_2 nanotube layers, whose photocurrent response disappeared at wavelengths higher than 400 nm, corresponding to the anatase bandgap of 3.2 eV.[3] Figure 4a shows that the Ti/TiO_2(1 μm)/CIS nanotube layers possess high *IPCE* values of about 25% at the visible light wavelength of 450 nm, and it remains quite robust at longer wavelengths (over 10% at 600 nm). In contrast, blank TiO_2 nanotube layers show *IPCE* only about 60% in the UV region (350 nm). As shown in Figure 4b, in the case of thicker nanotube layers, Ti/TiO_2 (6 μm), the blank TiO_2 nanotube layers show a *IPCE* of ≈30% in the UV region (350 nm) which is consistent with previous reports.[3,21] After coupling with CIS nanocrystals, a stronger sensitizing effect is observed for Ti/TiO_2(6 μm)/CIS nanotube layers in the UV as well as in the VIS light range. The Ti/TiO_2 (6 μm)/CIS nanotube layers possess high *IPCE* values, e.g. approximately 55% in the visible region (600 nm), and *IPCE* remains high at longer wavelengths (greater than 20% at 800 nm). The high *IPCE* values, in the case of 6 μm thick nanotube layers, correlates with the fact, that thicker TiO_2 nanotube layers with larger diameter (≈230 nm) can host more infilled visible light absorbing CIS nanocrystals compared to the ≈1 μm thick nanotube layers. The *IPCE* results obtained especially for 6 μm thick nanotube layers infilled with CIS are very promising and clearly show that TiO_2 nanotube layers infilled with CIS nanocrystals possess superior optical adsorption properties and incident photon to current conversion efficiency in the visible region of the solar spectrum. The enhanced UV response of the CIS infilled 6 μm thick nanotube layers can be most likely ascribed to the presence of chalcogen (Se) within the TiO_2 nanotubes.[22] This chalcogen heals out electron traps on the surface of the TiO_2 nanotubes, which provides significant contribution to the increased *IPCE* value. It is also noteworthy that similar improved UV light response was also observed in our previous work for sensitization of nanotube layers by As_3S_7.[11c]

In order to demonstrate the stability of CIS in 0.1 M aqueous Na_2SO_4 electrolyte used for the photoelectrochemical measurements, repeated cyclic voltammetry (CV) curves were recorded upon dark and light (wavelength 600 nm) conditions with a sweep rate of 50 mV/s in the voltage range from −0.4 to 0.8 V. One can see from the Figure 4c (under dark) and 4d (under light) that the CV curves do not change. This is positive and it indicates that CIS does not suffer from the anodic (cathodic) dissolution during the photocurrent experiments or at least the degradation of CIS seems to be negligible. The semiconducting nature of the TiO_2/CIS heterostructure makes it appropriate for the development of hybrid photoelectrochemical cells.

Figure 5 illustrates the transfer mechanism of photo-generated electrons at the Ti/TiO_2/CIS nanotubular interface.

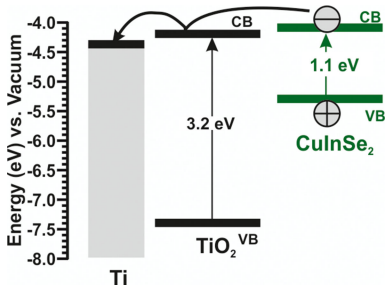

Figure 5. Schematic illustration of the energy levels of Ti/TiO_2/CIS heterojunction, and photo-generated electrons separation, and transport across the interface.

The TiO_2/CIS assembly forms a type II heterojunction where both the valence and the conduction bands of CIS are higher than those of TiO_2. Therefore, during the process of visible light photon harvesting, conduction-band electrons from CIS can migrate into the conduction band of TiO_2 which is driven by the energy levels difference, between the two conduction band edges.[13,23] The energy difference of the molecular orbitals can regulate the charge transfer path at the semiconductor interface, similarly as it does in case of dye-sensitized[7] and perovskite based solar cells.[24]

In conclusion, we have demonstrated that a simple electrodeposition technique can be used to quantitatively infiltrate CIS into the self-organized TiO_2 nanotube layers with different aspect ratios. The nanotubular bulk heterojunction of n-type TiO_2 and CIS displayed favourable visible light absorption ability, photo-generated charge separation, and transport performance that has not been demonstrated yet. The selection of TiO_2 nanotubes with different dimensions and electrochemical deposition of CIS for different times, led to significant photoelectrochemical performance of Ti/TiO_2/CIS electrodes, unseen before. In view of the facile and low cost electrodeposition fabrication route, we believe that such a method can provide a promising means for fabricating solid-state solar cells, utilizing n-type TiO_2 and p-type CIS materials.

Experimental Section

Clean Ti foils (Sigma-Aldrich, 0.127 mm, 99.7% purity) were anodized at room temperature using a high-voltage potentiostat (PGU-200 V, IPS Elektroniklabor GmbH) to fabricate two different types of TiO_2 nanotube layers: 1) ≈1 μm thick nanotube layers with ≈100 nm diameter (glycerol based electrolyte containing 50% water and 0.27 M NH_4F, 20 V),[25] marked as Ti/TiO_2(1 μm) and 2) ≈6 μm thick nanotube layers with ≈230 nm diameter (ethylene glycol based electrolyte containing 10% water and 0.15 M NH_4F, 100 V) marked as Ti/TiO_2(6 μm).

Electrodeposition was employed to load CIS nanoclusters into the TiO_2 nanotube layers to fabricate a functional composite structure. Prior to the electrodeposition of CIS, the TiO_2 nanotubes were annealed at 400 °C, to provide crystalline nanotubes, and to improve their electrical conductivity.[26] CIS electrodeposition was carried out using the standard three-electrode system, with a Pt counter electrode and Ag/AgCl as the reference electrode. A computer-controlled potentiostat (Autolab PGSTAT 204) was used for the electrochemical deposition. The CIS deposition solutions contained 2 mM $CuSO_4{\cdot}5H_2O$ (Aldrich, 97%), 4 mM H_2SeO_3 (Aldrich, 99.999%), and 4 mM $In_2(SO_4)_3{\cdot}4H_2O$ (Aldrich, ultrapure) in deionized water. The deposition voltage was in the range of −0.8 V vs Ag/AgCl electrode. The electrodeposition experiments were carried out for 780 s and 1560 s, for the Ti/TiO_2(1 μm) and Ti/TiO_2(6 μm), respectively, following a procedure described by Dharmadasa et al.[27] After the electrodeposition, the Ti/TiO_2/CIS heterostructures were annealed in a Se atmosphere at 450 °C for 10 min, to improve the crystallinity of the CIS electrodeposits. For the structural and morphological characterization of the anodized samples, top-view and cross-sectional observations were carried out by a field-emission electron microscope (FE-SEM JEOL JSM 7500F). The cross-sectional images were obtained from a mechanically bent sample, where a lift of the nanotube layer occurred. Diffraction analyses were also carried out using X-ray diffractometer (D8 Advance, Bruker AXE) using Cu $K\alpha$ radiation with secondary graphite monochromator and Na(Tl)I scintillation detector. Morphological and electron diffraction analyses were performed using a high resolution TEM microscope (ARM 200F, JEOL Ltd.) operated at 200 kV and equipped with EDX (Inca, Oxford Instruments).

A photocurrent spectroscopy system (Instytut Fotonowy, Poland) equipped with a monochromatized Xe lamp (150 W) was used for determination of the photocurrent generation efficiency (incident photon to current conversion efficiency, *IPCE*) at various wavelengths from 300 to 800 nm. All photoelectrochemical measurements were performed with an electrochemical setup consisting of Autolab potentiostat. Measurements were carried out in an aqueous solution of 0.1 M Na_2SO_4 (at 0.4 V vs. Ag/AgCl) in a three-electrode cell equipped with a flat quartz window. The electrodes were contacted and then pressed against an O-ring of a photoelectrochemical cell leading to an irradiated sample area of 0.28 cm^2. A platinum wire served as a counter electrode and Ag/AgCl (3 M KCl) as a reference electrode.

The *IPCE* for each wavelength was calculated according to Equation (1):

$$IPCE = \frac{i_{ph} h\nu}{Pq} \times 100 \quad (1)$$

where, i_{ph} is the photocurrent density, h is Planck's constant, ν is the irradiation frequency, P is the light power density, and q is the charge of an electron. The value of photocurrent density was taken as a difference between current density under irradiation and in the dark.

Acknowledgements

The European Research Council (ERC) and the Ministry of Education, Youth and Sports of the Czech Republic, are acknowledged for their financial support through projects 638857 and LM2015082, respectively. Associate Professor L. Benes is thanked for XRD measurements. Dr. Maria Caplovicova is thanked for TEM and EDX analyses.

Conflict of Interest

The authors declare no conflict of interest.

Keywords: anodization · heterostructures · TiO_2 nanotubes · incident photon-to-electron conversion efficiency · $CuInSe_x$

[1] a) V. Zwilling, M. Aucouturier, E. Darque-Ceretti, *Electrochim. Acta* **1999**, *45*, 921–929; b) P. Roy, S. Berger, P. Schmuki, *Angew. Chem. Int. Ed.* **2011**, *50*, 2904–2939; c) J. M. Macak, M. Zlamal, J. Krysa, P. Schmuki, *Small* **2007**, *3*, 300–304; d) K. Lee, R. Kirchgeorg, P. Schmuki, *J. Phys. Chem. C* **2014**, *118*, 16562–16566.

[2] a) J. M. Macak, H. Tsuchiya, A. Ghicov, K. Yasuda, R. Hann, S. Bauer, P. Schmuki, *Curr. Opin. Solid State Mater. Sci.* **2007**, *11*, 3–18; b) H. Sopha, L. Hromadko, K. Nechvilova, J. M. Macak, *J. Electroanal. Chem.* **2015**, *759*, 122–128; c) K. Lee, A. Mazare, P. Schmuki, *Chem. Rev.* **2014**, *114*, 9385–9454.

[3] a) R. Beranek, H. Tsuchiya, T. Sugishima, J. M. Macak, L. Taviera, S. Fujimoto, H. Kisch, P. Schmuki, *Appl. Phys. Lett.* **2005**, *87*, 243114–243116; b) R. Beranek, J. M. Macak, M. Gartner, K. Meyer, P. Schmuki, *Electrochim. Acta* **2009**, *54*, 2640–2646.

[4] S. U. M. Khan, M. Al-Shahry, W. B. Ingler Jr., *Science* **2002**, *297*, 2243–2245.

[5] S. Sato, *Chem. Phys. Lett.* **1986**, *123*, 126–128; R. Asahi, T. Morikawa, T. Ohwaki, K. Aoki, Y. Taga, *Science* **2001**, *293*, 269–271.

[6] T. Umebayashi, T. Yamaki, H. Itoh, K. Asai, *Appl. Phys. Lett.* **2002**, *81*, 454–456; T. Ohno, *Water Sci. Technol.* **2004**, *49*, 159–163.

[7] a) M. Gratzel, *Nature*, **2001**, *414*, 338–344; b) J. M. Macak, H. Tsuchiya, A. Ghicov, P. Schmuki, *Electrochem. Commun.* **2005**, *7*, 1133–1137; c) S. So, I. Hwang, P. Schmuki, *Energy Environ. Sci.* **2015**, *8*, 849–854.

[8] a) R. Vogel, P. Hoyer, H. Weller, *J. Phys. Chem.* **1994**, *98*, 3183–3188; b) W. T. Sun, W. T. , Y. Yu, H. Y. Pan, X. F. Gao, Q. Chen, L. M. Peng, *J. Am. Chem. Soc.* **2008**, *130*, 1124–1125; c) D. R. Baker, P. V. Kamat, *Adv. Funct. Mater.* **2009**, *19*, 805–811.

[9] M. Miyashita, K. Sunahara, T. Nishikawa, Y. Uemura, N. Koumura, K. Hara, A. Mori, T. Abe, E. Suzuki, S. Mori, *J. Am. Chem. Soc.* **2008**, *130*, 17874–17881.

[10] B. F. Silva, T. Andreani, A. Gavina, M. N. Vieira, C. M. Pereira, T. Rocha-Santos, R. Pereira, *Aquat. Toxicol.* **2016**, *176*, 197–207.

[11] a) A. Chiril, S. Buecheler, F. Pianezzi, P. Bloesch, C. Gretener, A. R. Uhl, C. Fella, L. Kranz, J. Perrenoud, S. Seyrling, R. Verma, S. Nishiwaki, Y. E. Romanyuk, G. Bilger, A. N. Tiwari, *Nat. Mater.* **2011**, *10*, 857–861; b) L. A. Burton, A. Walsh, *Appl. Phys. Lett.* **2013**, *102*, 132111–3; c) J. M. Macak, T. Kohoutek, L. Wang, R. Beranek, *Nanoscale* **2013**, *5*, 9541–9545; d) Y. Aida, V. Depredurand, J. K. Larsen, H. Arai, D. Tanaka, M. Kurihara, S. Siebentritt, *Prog. Photovolt: Res. Appl.* **2015**, *23*, 754–764; e) B. Saparov, J. P. Sun, W. Meng, Z. Xiaao, H. S. Duan, O. Gunawan, D. Shin, I. G. Hill, Y. Yan, D. B. Mitzi, *Chem. Mater.* **2016**, *28*, 2315–2322.

[12] a) D. B. Mitzi, *Adv. Mater.* **2009**, *21*, 3141–3158; b) M. E. Norako, R. L. Brutchey, *Chem. Mater.* **2010**, *22*, 1613–1615; c) C. J. Stolle, T. B. Harvey, D. R. Pernik, J. I. Hibbert, J. Du, D. J. Rhee, V. A. Akhavan, R. D. Schaller, B. A. Korgel, *J. Phys. Chem.: A* **2014**, *5*, 304–309.

[13] Z. Zhou, J. Fan, X. Wang, W. Sun, W. Zhao, Z. Du, S. Wu, *ACS Appl. Mater. Interfaces* **2011**, *3*, 2189–2194.

[14] a) Y. Liao, H. Zhang, Z. Zhong, L. Jia, F. Bai, J. Li, P. Zhong, H. Chen, J. Zhang, *ACS Appl. Mater. Interfaces* **2013**, *5*, 11022–11028; b) Q. Wang, J. Qiao, J. Zhou, S. Gao, *Electrochim. Acta* **2015**, *167*, 470–475.

[15] Z. Wu, X. Tong, P. Sheng, W. Li, X. Yin, J. Zou, Q. Cai, *Appl. Surf. Sci.* **2015**, *351*, 309–315.
[16] a) P. Sheng, W. Li, X. Tong, X. Wang, Q. Cai, *J. Mater. Chem. A*, **2014**, *2*, 18974–18987; b) P. Sheng, W. Li, X. Wang, X. Tong, Q. Cai, *ChemPlusChem* **2014**, *79*, 1785–1793.
[17] a) J. M. Macak, B. G. Gong, M. Hueppe, P. Schmuki, *Adv. Mater.*, **2007**, *19*, 3027–3031; b) H Zhang, X. Quan, S. Chen, H. Yu, N. Ma, *Chem. Mater.* **2009**, *21*, 3090–3095; c) J. M. Macak, C. Zollfrank, B. J. Rodriguez, H. Tsuchiya, M. Alexe, P. Greil, P. Schmuki, *Adv. Mater.* **2009**, *21*, 3121–3125; d) Q. Kang, Q. Cai, S. J. Yao, C. A. Grimes, J. Ye, *J. Phys. Chem. C* **2012**, *116*, 16885–16892; e) Y. Gim, M. Seong, Y. W. Choi, J. Choi, *J. Electochem. Commun.* **2015**, *52*, 37–40.
[18] D. Routkevitch, T. Bigioni, M. Moskovits, J. M. Xu, *J. Phys. Chem.* **1996**, *100*, 14037–14047.
[19] Q. Wang, K. Zhu, N. R. Neale, A. J. Frank, *Nano. Lett.* **2009**, *9*, 806–813.
[20] S. Ishizuka, A. Yamada, P. J. Fons, H. Shibata, S. Niki, *Progr. Photovolt.* **2014**, *22*, 821–829.
[21] Q. Liu, J. He, T. Yao, Z. Sun, W. Cheng, S. He, Y. Xie, Y. Peng, H. Cheng, Y. Sun, Y. Jiang, F. Hu, Z. Xie, W. Yan, Z. Pan, Z. Wu, S. Wei, *Nat. Commun.* **2014**, *5*, 5122–5129.
[22] a) J. W. Zheng, A. Bhattcahrayya, P. Wu, Z. Chen, J. Highfield, Z. Dong, R. Xu, *J. Phys. Chem C* **2010**, *114*, 7063–7079; b) T. Umebayashi, T. Yamaki, H. Itoh, K. Asai , *Appl. Phys. Lett.* **2002**, *81*, 454–456.
[23] a) T. L. Li, H. Teng, *J. Mater. Chem.* **2010**, *20*, 3656–3664; b) D. A. Gaal, J. T. Hupp, *J. Am. Chem. Soc.* **2000**, *122*, 10956–10963.
[24] a) A. Kojima, T. Teshima, Y. Shirai, T Miyasaka, *J. Am. Chem. Soc.* **2009**, *131*, 6050–6051; b) X. Gao, J. Li, J. Baker, Y. Hou, D. Guan, J. Chen, C. Yuan, *Chem. Commun.* **2014**, *50*, 6368–6371.
[25] J. M. Macak, H. Hildebrand, U. Marten-Jans, P. Schmuki, *J. Electroanal. Chem.* **2008**, *621*, 254–266.
[26] S. Das, R. Zazpe, J. Prikryl, P. Knotek, M. Krbal, H. Sopha, V. Podzemna, J. M. Macak, *Electrochim. Acta* **2016**, 213, 452–459.
[27] I. M. Dharmadasa, R. P. Burton, M. Simmonds, *Sol. Energy Mater. Sol. Cells* **2006**, *90*, 2191–2200.

Manuscript received: November 28, 2016
Accepted Article published: January 15, 2017
Final Article published: February 8, 2017